
High-Resolution PET Imaging for In Vivo Monitoring of Tumor Response After Photodynamic Therapy in Mice

David Lapointe, Nicole Brasseur, Jules Cadorette, Carole La Madeleine, Serge Rodrigue, Johan E. van Lier and Roger Lecomte

Centre d'Imagerie Métabolique et Fonctionnelle, Clinical Research Center, Department of Nuclear Medicine and Radiobiology, Faculty of Medicine, Université de Sherbrooke, Sherbrooke, Quebec, Canada

The aim of this study was to investigate the use of [^{18}F]fluoro-2-deoxy-D-glucose (FDG) and a small-animal PET scanner to assess early tumor response after photodynamic therapy (PDT) in mice. PDT consists of intravenous administration of a photosensitizer that accumulates preferentially in tumor tissue, followed by local illumination of the tumor with red light. Two different photosensitizers were used: Photofrin (PII), which has been approved for clinical use, and disulfonated aluminum phthalocyanine (AIPcS), which is a second-generation drug. These drugs have been shown to induce tumor necrosis through different action mechanisms, i.e., mainly initial vascular stasis (PII) or direct tumor cell kill (AIPcS). FDG PET was used to follow both perfusion and metabolic activity in the tumor tissue. **Methods:** The study was performed using a mouse model implanted with two contralateral murine mammary tumors (5 mm diameter \times 2.5 mm thickness) on the back. Only one tumor was subjected to PDT, whereas the other tumor served as a control. A total of 13 mice were studied, 1 without illumination, 3 at 30 min and 3 at 2 h after PDT with both PII-PDT and AIPcS-PDT. Dynamic PET imaging of the mice, which were placed in pairs in a prostate position parallel to the transaxial planes of the Sherbrooke animal PET scanner, was performed after a bolus injection of 11 MBq (300 μCi) FDG. Blood samples were collected concurrently from 1 mouse during each study using an automated microvolumetric blood sampler. **Results:** Analysis of the tumor time-activity curves showed that (a) scans during the first 3 min provided an estimate of tumor perfusion, as confirmed by the blood samples; (b) the tumor FDG uptake after 15 min was a direct measurement of tumor metabolism clearly demonstrating the relative efficacy of the two PDT drugs; and (c) the tumor tracer concentration in the interval 3–15 min after FDG injection is an appropriate indicator of the different mechanisms of tumor necrosis through indirect vascular stasis (PII) or direct cell kill (AIPcS). **Conclusion:** This pilot study confirmed the feasibility of using dynamic in vivo PET imaging for assessing early tumor response to PDT in mice.

Key Words: PET; fluorodeoxyglucose; photodynamic therapy; tumor response

J Nucl Med 1999; 40:876–882

PET permits the in vivo quantification of positron-emitting tracers, thus providing a dynamic picture of the distribution of a radiopharmaceutical over time. Such direct measurement of the time course of radiotracers has been used to investigate a variety of physiological and biochemical processes, including blood flow and perfusion, metabolism, protein synthesis and receptor-specific ligands (1–3). Until recently, quantitative PET studies were limited mostly to humans or large animals because of the poor spatial resolution of existing clinical PET scanners (4–6). The development of high-resolution PET scanners dedicated to small-animal imaging (7–12) now makes it possible to consider these methodologies for research applications in laboratory animal models. Indeed, PET has the potential to supplant the classic dissection-based approaches in a number of pharmaceutical and physiological research studies (13). A specific advantage of PET is the ability to perform fast, dynamic studies in the same animal, which allows consistent kinetic data to be gathered regardless of interanimal variability. Another advantage of PET is the possibility of performing repeated measurements in the same animal over extended periods, thus allowing longitudinal and follow-up studies. One such application of PET in animal research deals with the evaluation of tumor metabolism and response to therapy.

Photodynamic therapy (PDT) is a new treatment modality for solid tumors. The procedure consists of the administration of a photosensitizer that accumulates preferentially in the tumor, followed by the local illumination of neoplastic tissues with red light (reviews, 14–16). The light absorption by the photosensitizer results in the formation of a variety of activated oxygen and radical species, which initiate a cascade of biochemical reactions leading to microvascular collapse as well as direct tumor cell kill, resulting in tumor necrosis and eventually cure (17). The rapid response of tumors to PDT may result, in part, from the rapid and efficient induction of apoptosis and from cell necrosis (18,19).

Photofrin (PII; QLT Phototherapeutics, Inc., Vancouver,

Received Mar. 24, 1998; revision accepted Oct. 18, 1998.
For correspondence or reprints contact: Roger Lecomte, PhD, CRC/CIMF, Department of Nuclear Medicine and Radiobiology, Université de Sherbrooke, 3001 12th Ave. N., Sherbrooke, Quebec, Canada J1H 5N4.

British Columbia, Canada), a mixture of hematoporphyrin derivatives, was approved in 1995 in the U.S., Canada, Japan and several European countries for clinical PDT of selected cancers, including early lung cancer (20). However, this photosensitizer preparation presents several disadvantages, notably chemical heterogeneity, low absorption of tissue-penetrating red light and long-term cutaneous photosensitivity (21). In the search for improved second-generation photosensitizers, phthalocyanines (PcSs) have been proposed (22–24). Compared with porphyrins, these dyes offer a higher molar extinction coefficient at a red-shifted absorption maximum of approximately 680 nm, which results from the condensation of benzene rings to the periphery of their porphyrin-like macrocycle. Phthalocyanines form stable chelates with metal cations, and the biologic potential of the water-soluble gallium, aluminum and zinc-sulfonated phthalocyanine has been well documented. We have previously shown that among differently sulfonated phthalocyanines (PcSs), the amphiphilic dye-bearing sulfonate groups on two adjacent benzene rings exhibits optimal *in vitro* phototoxicity (25) because of better cell-penetrating properties (26) and targeting of photosensitive intracellular sites (27,28). In contrast to PII, for which PDT efficacy is mostly mediated by indirect effects on the tumor microvasculature, amphiphilic disulfonated aluminum phthalocyanine (AlPcS) induces tumor necrosis with fewer vascular effects. The existence of different mechanisms of action of these two types of photosensitizers is supported by histopathological findings (29) as well as measurement of tumor vascular effects (30,31) and tumor cell survival after PDT (32). Previously, we used tracer techniques to quantify the effect of PDT on the tumor vasculature by using the clinical perfusion agent ^{99m}Tc-hexakis-2-methoxyisobutyl isonitrile (MIBI) (33). The potential to use [¹⁸F]fluoro-2-deoxy-D-glucose (FDG) PET to monitor tumor glucose metabolism after PII-PDT in an animal model has recently been demonstrated (34). In this study, we evaluated the use of FDG and animal PET to measure tumor response after PDT in mice, both in terms of changes in perfusion rates and metabolic activity. In addition to confirming the usefulness of animal PET in assessing the efficacy of an experimental cancer treatment modality, this study allowed us to evaluate the potential of FDG PET to quantify the involvement of different action mechanisms associated with specific treatment protocols leading to tumor regression.

MATERIALS AND METHODS

Photosensitizers

Lyophilized PII was supplied by QLT Phototherapeutics, Inc. and was reconstituted with 30 mL dextrose (5%) in sterile water to obtain a concentration of 2.5 mg/mL. Aliquots were frozen and further diluted in dextrose (5%) at the time of use, according to the recommendations of the supplier. AlPcS, i.e., the disulfonated fraction enriched in isomers with sulfonate substituent on adjacent benzene rings, was prepared by the condensation method, as described previously (35), and formulated in an oil emulsion containing 10% Cremophor EL (Sigma, Mississauga, Ontario,

Canada) and 3% 1,2-propanediol (Sigma) in phosphate-buffered saline and then sterile filtered (0.2 μm). The dye concentration was determined by spectrophotometry after dilution in dimethyl formamide ($\epsilon_{680 \text{ nm}} = 250,000 \text{ M}^{-1} \text{ cm}^{-1}$). The working solution of AlPcS was prepared by diluting the stock solution in phosphate-buffered saline such that a 0.2-mL administered volume gave a 1-μmol drug dose.

Animal Model

All experiments were performed on male BALB/c mice (18–22 g) (Charles River Breeding Laboratories, Montreal, Quebec, Canada) bearing two EMT-6 mammary tumors. The experiments were conducted following a protocol approved by the Canadian Council on Animal Care and the in-house ethics committee. Animals were allowed free access to water and food throughout the experiments. Before tumor implantation, hair on the hind legs and the backs of the mice was removed by shaving and chemical depilating (Nair, Whitehall, Mississauga, Canada). The two tumors were implanted on the backs of the animals by intradermal injection of 2×10^5 EMT-6 cells suspended in 0.05 mL Waymouth's growth medium.

Photodynamic Therapy

For PDT studies, mice were used 17 d after tumor cell inoculation (mean external tumor size = 5 ± 1 mm diameter, 2.5 ± 0.5 mm thickness). The mice were given an intravenous administration of 5 mg/kg PII or 1 μmol AlPcS (0.2 mL/20 g) through the tail vein. These are the minimum administered doses required for these agents to inflict a similar level of tissue damage 3 d after PDT (32). After 24 h, one tumor was treated with an 8-mm beam of red light (200 mW/cm² for a total fluence of 400 J/cm²), whereas the other tumor served as a control. The light consisted of a broad band, 650–700 nm (AlPcS) or 600–650 nm (PII), generated by a 1000-W Xenon lamp, equipped with a 10-cm circulating water filter and two glass filters (Corion LL-650 and LS-700 or Corion LL-600 and LS-650; Corion Corporation, Franklin, MA).

PET Study

A total of 13 mice under ketamine-xylazine anesthesia were prepared with indwelling PE-10 catheters (inner diameter 0.28 mm, outer diameter 0.61 mm) in the jugular vein and administered with 75 USP heparin. Mice were then placed 2 by 2 in a prostate position on a polystyrene holder, allowing simultaneous imaging of 2 animals in a transversal plane. The position of the scanner bed was adjusted such that the mice were parallel to the transaxial planes and the four tumors were centered within the axial field of view (FOV) of the scanner with the help of a laser beam. At predetermined times after PDT treatment (30 min and 2 h), each mouse was injected intravenously with 11 MBq (300 μCi) FDG in a variable volume of 30–100 μL saline over a 30-s interval using an infusion pump and then chased with 100 μL saline. FDG was supplied by the Chedoke-McMaster Hospital cyclotron facility (Hamilton, Ontario, Canada). The specific activity varied between 18,500 GBq/μmol (500 Ci/μmol) and 2200 GBq/μmol (60 Ci/μmol) from the first to the last injection.

PET scans were obtained with the Sherbrooke high-resolution animal PET scanner, the first positron tomograph based on avalanche photodiode detectors (12,36). This scanner achieves a reconstructed resolution of 2.1 mm transaxially \times 3.1 mm axially, a sensitivity of 2600 cps/MBq (100 cps/μCi) for an axial line source in air at the center of FOV and a high noise effective sensitivity achieved through low random and scatter event rates (12). The following serial dynamic PET data were obtained, starting at the

beginning of FDG injection: 30 frames of 5 s, 34 frames of 20 s and 6 frames of 60 s. Static scans of 3 min with oversampling motion (36) were obtained at the end of the dynamic sequences for reconstruction at higher resolution on a grid of 256×256 pixels (0.95 mm/pixel). Accidental coincidences measured in a delayed time window were subtracted from the emission data, and the emission sinograms were subsequently normalized for counting efficiency. Image reconstruction was performed using the maximum likelihood expectation maximization reconstruction method with 30 iterations. For quantitative evaluation, regions of interest were defined in the medial portion of the tumors. Time-activity curves were generated and corrected for radionuclide decay.

Blood samples of 10 μ L were collected simultaneously with the help of a computer-controlled microvolumetric sampler (37,38) at 20, 30, 50 and 90 s and 5, 15, 25 and 40 min after injection of the radiotracer. A small section (6 μ L) of the implanted catheter connected to a "T" junction was used for both the injection of FDG and the blood sampling. The tubing was chased with 20 μ L saline after FDG injection and was counted in a gamma counter (Wallac model 1282; Wallac, Turku, Finland) to measure possible contamination after the experiment. Injecting air bubbles through a T connector created individual blood samples in the tubing. At the end of the experiment, the tubing containing the samples was measured, cut

and sealed at the bubbles separating the samples. Blood samples were then placed in test tubes and counted in the gamma counter. Measured activity was corrected for decay and sample volume. Blood glucose concentration was measured before FDG injection and at the end of scanning using a portable glucometer device.

Three mice were scanned for each photosensitizer and at each time post-PDT (30 min and 2 h) (12 in total). One control mouse injected with FDG and the photosensitizer but not illuminated was also scanned. In an earlier study, it was shown that the treatment with drug alone or light alone did not affect tumor perfusion and metabolism (32). At the end of the scanning, the mice were killed with a lethal injection of pentobarbital (25 mg) and kept frozen for histopathology of the tumor tissues. Twenty-four hours after the experiment, tumors and the surrounding tissues were removed and fixed in formol and then prepared for light microscopy. Sections of paraffin-embedded tissues were stained with hematoxylin and eosin. MRI was performed on different animals from 20 min to 2 h after PDT for comparison and identification purposes.

RESULTS

Figure 1 shows a typical example of the dynamic PET image series obtained in a mouse after injection of 11 MBq

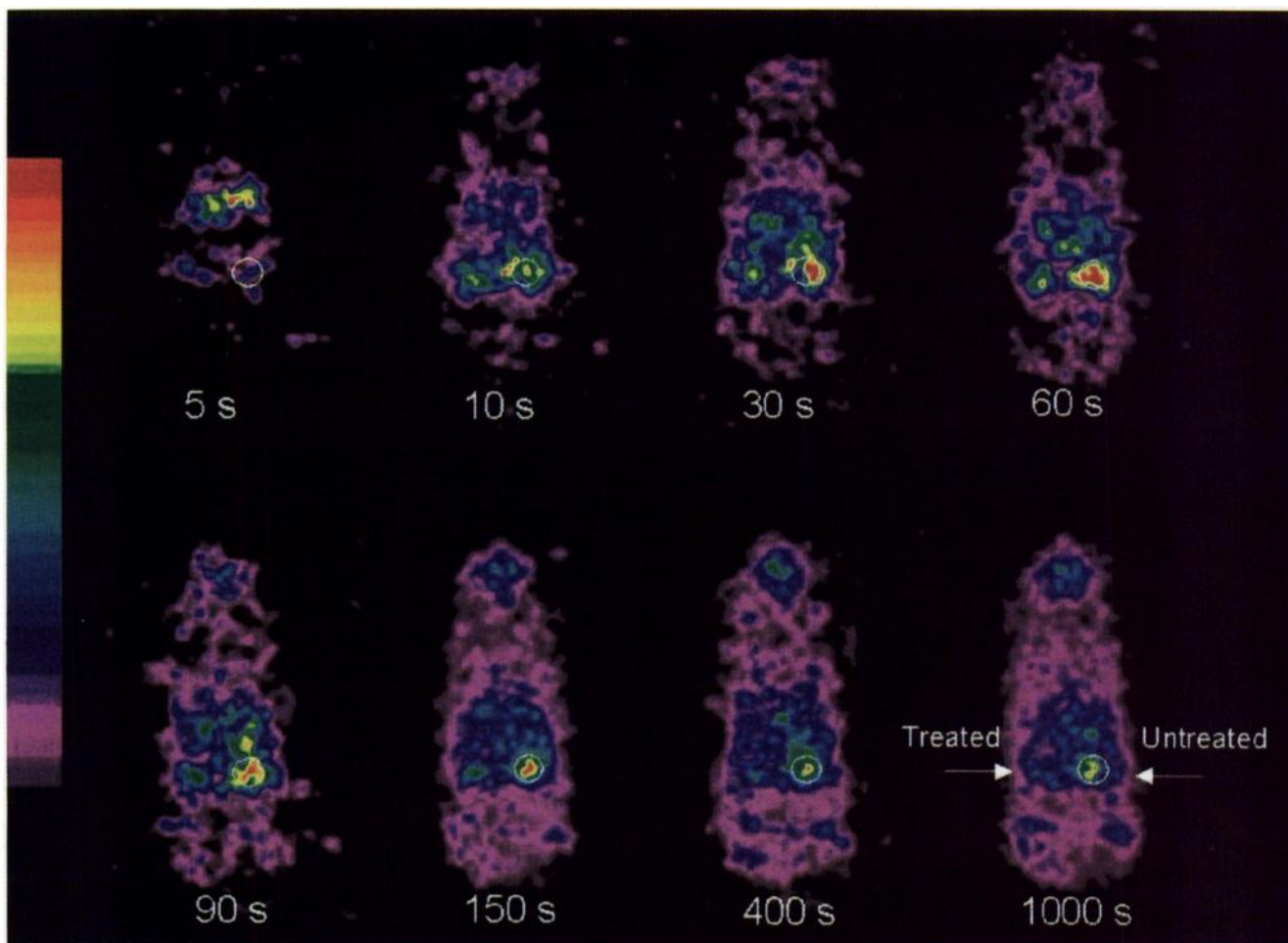


FIGURE 1. Dynamic image sequence shows accumulation of FDG after PII-PDT in mouse bearing two EMT-6 tumors. Animal was intravenously injected with 5 mg/kg PII; PDT was applied to left tumor only; and 2 h later, 11 MBq (300 μ Ci) FDG were intravenously injected for PET imaging. Right tumor (indicated by circle), which was not exposed to light treatment, shows normal delivery and accumulation of FDG, whereas uptake is significantly reduced in treated tumor (left arrow).

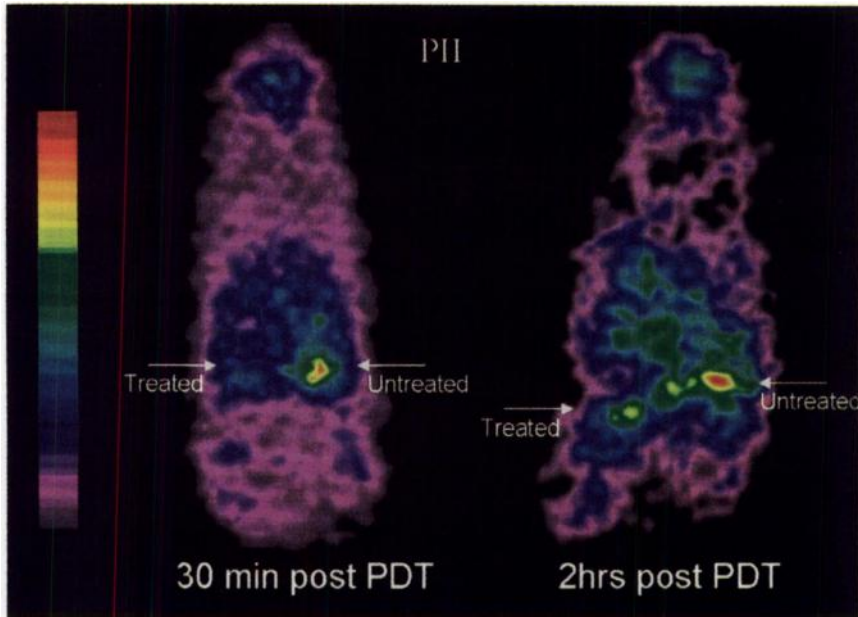


FIGURE 2. PET images of FDG biodistribution 30 min after administration in mice bearing two EMT-6 tumors; 1 mouse was treated with PII-PDT 30 min (left) and the other 2 h (right) before PET imaging.

(300 μ Ci) FDG. The first five images show the passage of activity into the blood compartment up to a peak between 30 and 60 s, corresponding to the end of injection. The following images show the gradual uptake of activity within tumor tissues. At 1800 s after start of injection of the radiotracer, a tumor-to-surrounding tissue radioactivity ratio of at least 10:1 is observed for the untreated tumors, whereas the uptake in the PDT-treated tumors is significantly lower, reflecting the effects of PDT on tumor metabolism. In contrast, the MR images did not show any detectable difference between the treated and untreated tumors over the entire time span (from 20 min to 2 h after PDT) during which image acquisition was performed (data not shown).

Figure 2 shows the FDG uptake in 2 mice 1800 s after injection, for administration of FDG at 30 min and 2 h

post-PDT with PII. Figure 3 shows the FDG uptake for AIPcS-PDT treated mice. The tumors treated with PII show a clear decrease in FDG accumulation compared with the control tumor at both 30 min and 2 h post-PDT (Fig. 2), indicating very early effects of PDT on tumor metabolism. In the case of AIPcS (Fig. 3), at 30 min after PDT, both control and treated tumors are visible, reflecting a different, slower action mechanism for this photosensitizer. However, at 2 h post-PDT, FDG activity in the treated tumor has diminished to a level comparable with that of the blood pool, indicating suppression of the tumor metabolic activity.

Figure 4 shows the time-activity curves of the FDG uptake in the treated and untreated tumors at 30 min and 2 h postirradiation with PII-PDT and AIPcS-PDT. Tumors from 1 control mouse (data not shown) and the unirradiated

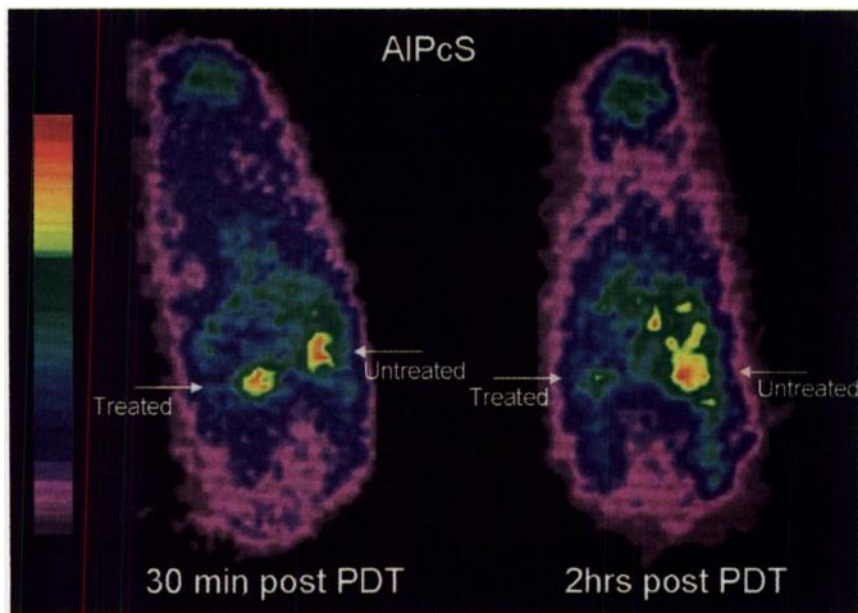


FIGURE 3. PET images of FDG biodistribution 30 min after administration in mice bearing two EMT-6 tumors; 1 mouse was treated with AIPcS-PDT 30 min (left) and the other 2 h (right) before PET imaging.

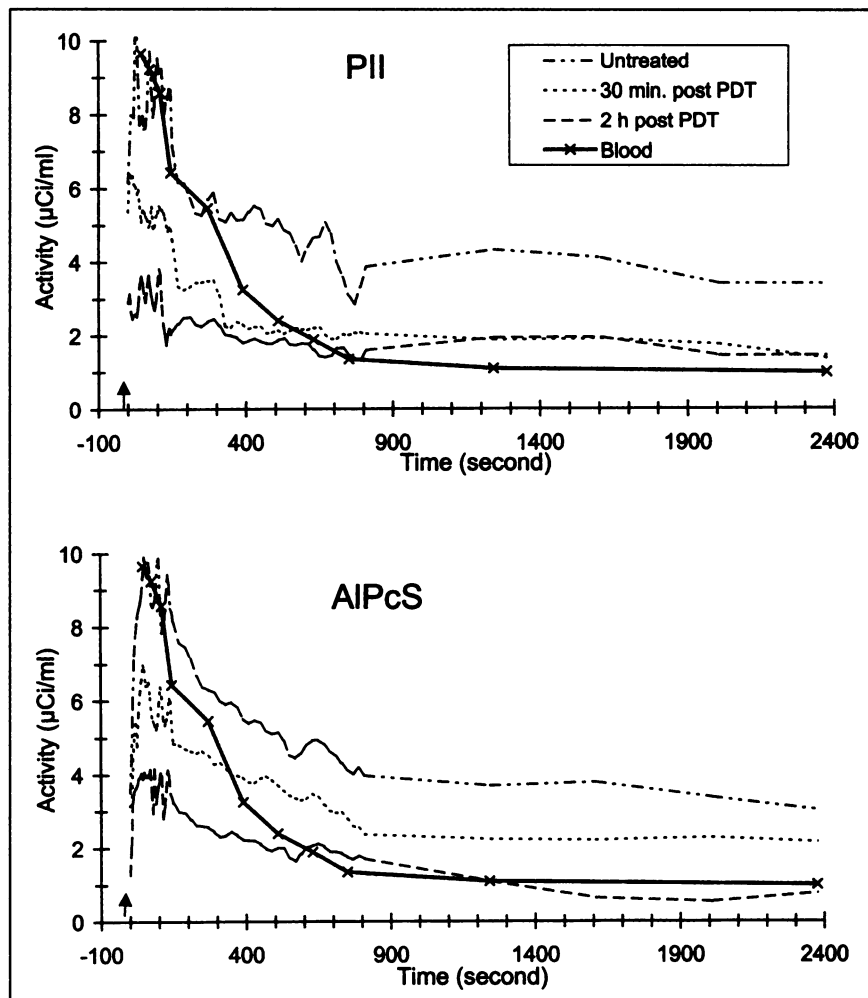


FIGURE 4. (Top) FDG tumor uptake in mice treated with PII-PDT. (Bottom) FDG tumor uptake in mice treated with AIPcS-PDT.

tumors from mice treated with PII or AIPcS show the same FDG uptake pattern. During the first 50–300 s immediately after FDG injection, the activity in untreated tumors parallels the blood activity, reflecting circulating FDG levels. Thereafter, tumor activity decreases less rapidly than blood activity, indicating FDG accumulation in the tumor. Because the overall observed activity in the untreated tumor represents residual FDG activity in the tumor blood pool and FDG taken up by the tumor cells, the difference in FDG concentration between the tumor and the blood can provide an estimate of the FDG actually retained by the tumor tissue. At steady state, which is reached at about 750 s after FDG injection, the activity level in the untreated tumor is taken as 100% cell survival.

In tumors treated with PII-PDT (Fig. 4, top), the initial FDG activity remains well below the control tumor and blood FDG levels, suggesting reduced blood flow and poor delivery of the tracer at the tumor site. This effect is even more accentuated at 2 h postirradiation, reflecting the extensive vascular damage that develops rapidly after PII-PDT, hindering tumor perfusion and, thus, FDG accumulation within the tumor tissue. At 30 min post-PDT, the FDG is washed out from the tumor at about the same rate as from the

blood, indicating that the tracer is poorly retained by the tumor. At 2 h, very little FDG is even delivered to the tumor. However, both curves level off slightly above the blood curve, indicating that some FDG is still accumulating in the tumor cells. Previous *ex vivo* studies using ^{99m}Tc -MIBI showed that tumor vascular perfusion dropped from 60% immediately after PII-PDT to as low as 20% at 2 h post-PDT relative to control tumors (32). The extensive vascular effect on tumors treated by PII-PDT was further confirmed by histopathological examination, as previously reported (29).

In tumors treated with AIPcS-PDT (Fig. 4, bottom), at 30-min post-PDT, FDG uptake at steady state falls to about 50% of the control value while remaining well above the blood activity level. In contrast, at 2 h postirradiation, tumor activity drops to the blood activity level. These results are consistent with an action mechanism proceeding primarily by initial direct cell kill, resulting in a gradual decrease in tumor cell survival while sparing tumor microvasculature (32). Using colony formation assays, it was previously shown that 80% of the tumor cells are inactivated with this treatment protocol at 2 h post-PDT. Therefore, the low FDG tumor activity found at 2 h post-PDT likely reflects the presence of an important fraction of dead cells. Histological

observations of tumors treated by AIPcS-PDT also showed a large number of pycnotic cells but less damage to the vasculature (29).

With both PDT drugs, FDG uptake in the tumors at 2 h post-PDT is low, indicating that significant damage has occurred in the tumor tissue. However, differences in the early dynamic uptake pattern of FDG correlate with distinct differences in the action mechanism of PDT, which subsequently led to tumor regression in both cases. The more rapid drop of FDG in tumors treated with PII-PDT at 30-min post-PDT indicates an early destruction of the tumor vascular system. In contrast, the more progressive decrease of tumor activity in AIPcS-PDT-treated tumors reflects the initial integrity of the microvasculature and is supportive of a high rate of direct inactivation of tumor cells.

DISCUSSION

The Sherbrooke animal PET scanner has a volume resolution of about 0.015 mL. Given the small size of the tumors in the mouse model used in this study (~0.05 mL), partial volume and spillover effects can be substantial and may prevent direct absolute quantification of the radiotracer concentration. To minimize these problems, the tumors were implanted as far as possible from the bladder and kidneys to limit spillover, and regions of interest of the same size (2-mm diameter) were placed in the central region of the tumors to compensate for the effect of partial volume when comparing tumor activities. In PII-treated mice, edema induced by vasodestruction in the treated tumor may affect the control tumor, which can be observed visually in Fig. 3, at 2 h post-PDT.

The heterogeneity of the tumors, which incorporate a rich vascularization, makes it difficult to discriminate FDG activity accumulated in tumor tissues from that flowing through the blood vessels. As a consequence, the radiotracer quantification in the region of interest represents not only tumor metabolism but also tumor blood flow and perfusion. This feature is clearly visible in the time-activity curves shown in Figure 4. In the first few minutes after FDG administration, the radiotracer activity in untreated tumors closely parallels that in the collected blood samples, indicating that circulating FDG in the blood mostly determines the observed tumor activity. After about 300 s, the increasing difference between the two curves is indicative of tumor perfusion while blood activity is being washed out. After about 750 s, when most activity has disappeared from the blood, the region-of-interest activity mostly represents FDG accumulation in tumor cells. Therefore, the lower initial FDG activity observed for the treated tumors can be directly related to a lack of blood supply and tumor perfusion resulting from vascular damage. Conversely, the lower activity observed at a later time after radiotracer administration reflects reduced tumor uptake caused by cell death.

The FDG PET studies clearly demonstrate the effects of PDT on tumors shortly after treatment. This is in sharp contrast with simple imaging visual examination of the tumors or other anatomic imaging modalities (e.g., MRI, CT) that can

detect only macroscopic damage normally appearing at a much later time after therapy (29). Investigation of the treatment efficacy at the tissue level with classical methods requires a large number of animals and is labor intensive. The *in vivo* and real-time capability of PET allowed us to investigate tumor response on a much shorter time scale, using only a few subjects. Furthermore, the ability of the animal PET scanner to acquire fast, dynamic image series enabled us to obtain additional information pertaining to differences in action mechanisms between different tumor treatment protocols. The fast, short-time, dynamic image frames obtained in the first few minutes after injection of FDG provided data for the assessment of tumor perfusion. For FDG PET at 2-h post-PDT, both PII-PDT and AIPcS-PDT were found to result in low tumor perfusion and low FDG uptake, reflecting collapse of the tumor vascular system and extensive tissue damage, in agreement with previously reported cell survival and histopathological data (29,32). For FDG PET at 30 min after treatment, however, the study demonstrates a more rapid effect of PII-PDT, as evidenced by the steeper initial descent of the total tumor activity and lower FDG uptake. In contrast, the activity in tumors treated with AIPcS-PDT decreases more slowly and reaches a plateau at about 50% of the control value. These differences in the time-activity curves are consistent with the distinct, prominent action mechanisms of these photosensitizing drugs, as previously demonstrated with ^{99m}Tc-MIBI to assess tumor vascular perfusion (33) and a colony formation assay to measure cell survival (32). At 30 min after PII-PDT, the drop of tumor activity to the baseline is a consequence of the abrupt vasoconstriction and early microvascular damage induced by PDT, which prevent uptake of the FDG by the tumor cells. It is the lack of blood supply that subsequently leads to indirect cell killing. On the contrary, the slow decrease of FDG activity after AIPcS-PDT is consistent with a direct cell-killing mechanism that does not initially affect microvascularization (Fig. 4, bottom: the 30-min post-PDT time-activity curve is parallel to that of the control), thus allowing FDG to penetrate the tumor tissues. Blood circulation is then progressively impaired because of tumor necrosis.

PDT is known to cause most of the tumor damage in the first few hours postillumination as a result of biochemical and physiologic modifications affecting both the tumor and the surrounding tissues. Dynamic PET imaging of FDG yields an estimate of glucose metabolism, a process that is being disturbed by these physiologic and biochemical changes. As a consequence, both the kinetics of FDG and the dynamics of the PDT response must be taken into account in interpreting the time-activity curves obtained in these experiments. Such mixed processes are difficult to model and make the analysis of the results particularly complex. In addition, the FDG time-activity curves were obtained only at two specific times after treatment (30 min and 2 h), making it difficult to reconstruct the full sequence of events immediately after tumor treatment. However, PET imaging can be easily modified to perform serial studies highlighting spe-

cific aspects of the PDT mechanisms immediately after illumination or to assess tumor response by reevaluating cell survival at later times (days) after treatment. For instance, shorter half-life radiotracers such as ^{11}C -methionine or ^{15}O - H_2O could be used with successive injections to evaluate modifications of tumor blood flow and perfusion immediately after PDT. Moreover, FDG could be used to repeatedly monitor treatment outcome at later times. The efficiency of fractionated illumination during PDT could also be investigated to develop more efficient treatment protocols. Alternatively, the PDT drugs could be labeled with a suitable radiotracer to determine the optimal illumination time after administration (39).

CONCLUSION

We have demonstrated the feasibility and suitability of FDG PET to study tumor response after photodynamic treatment in a small-animal model. The approach proved to be particularly useful for investigating early tumor response and mechanistic phenomena immediately after PDT. Dynamic, high-resolution, small-animal PET has been shown to be a unique tool to provide information on the action mechanisms of photosensitizing drugs, but it is also obvious that it can be used as a rapid screening procedure for selecting new drugs and for optimizing treatment protocols.

ACKNOWLEDGMENTS

We thank Dr. Christian Blais (Department of Radiology, Université de Sherbrooke) for access to the MRI scanner. This study was partially supported by the Medical Research Council of Canada.

REFERENCES

- Hawkins RA, Hoh C, Glaspy J, et al. The role of positron emission tomography in oncology and other whole-body applications. *Semin Nucl Med.* 1992;XXII:268–284.
- Phelps ME, Mazziotta JC, Schelbert HR. *Positron Emission Tomography and Autoradiography.* New York, NY: Raven Press; 1986.
- Reivich M, Alavi A. *Positron Emission Tomography.* New York, NY: Alan R. Liss; 1985.
- Ingvar M, Eriksson L, Rogers GA, Stone-Elander S, Widén L. Rapid feasibility studies of tracers for positron emission tomography: high-resolution PET in small animals with kinetic analysis. *J Cereb Blood Flow Metab.* 1991;11:926–931.
- Heiss W-D, Wienhard K, Graf R, Lottgen J, Pietrzyk U, Wagner R. High-resolution PET in cats: application of a clinical camera to experimental studies. *J Nucl Med.* 1995;36:493–498.
- Cutler PD, Cherry SR, Hoffman EJ, Digby WM, Phelps ME. Design features and performance of a PET system for animal research. *J Nucl Med.* 1992;33:595–604.
- Bloomfield PM, Rajeswaran S, Spinks TJ, et al. The design and physical characteristics of small animal positron emission tomograph. *Phys Med Biol.* 1995;40:1105–1126.
- Cherry SR, Shao Y, Silverman RW, et al. MicroPET: a high resolution PET scanner for imaging small animals. *IEEE Trans Nucl Sci.* 1997;44:1161–1166.
- Bruyndonckx P, Liu X, Tavernier S, Zhang S. Performance study of a 3D small animal PET scanner based on BaF_2 crystals and a photo sensitive wire chamber. *Nucl Instrum Meth Phys Res.* 1997;A392:407–413.
- Watanabe M, Uchida H, Okada H, et al. A high resolution PET for animal studies. *IEEE Trans Med Imaging.* 1992;11:577–580.
- Watanabe M, Okada H, Shimizu K, et al. A high resolution animal PET scanner using compact PS-PMT detectors. *IEEE Trans Nucl Sci.* 1997;44:1277–1282.
- Lecomte R, Cadorette J, Rodrigue S, et al. Initial results from the Sherbrooke avalanche photodiode positron tomograph. *IEEE Trans Nucl Sci.* 1996;43:1952–1957.
- Hichwa R. Are animal scanners really necessary for PET? [editorial]. *J Nucl Med.* 1994;35:1396–1397.

- Dougherty TJ. Photodynamic therapy. *Photochem Photobiol.* 1993;58:895–900.
- Fisher AM, Murphree AL, Gomer CJ. Clinical and preclinical photodynamic therapy. *Lasers Surg Med.* 1995;17:2–31.
- Kessel D. Photodynamic therapy of neoplastic disease. *Drugs Today.* 1996;32:385–396.
- Henderson BW, Dougherty TJ. How does photodynamic therapy work? *Photochem Photobiol.* 1992;55:145–157.
- Chuannong Z, Chi S, Deng J, et al. Apoptosis of mouse MS-2 fibrosarcoma cells induced by photodynamic therapy with Zn(II) -phthalocyanine. *J Photochem Photobiol B.* 1996;33:219–223.
- Zaidi Syed IA, Oleinick NL, Tarif Zaim M, Muktar H. Apoptosis during photodynamic therapy-induced ablation of RIF-1 tumors in C3H mice: electron microscopic, histopathologic and biochemical evidence. *Photochem Photobiol.* 1993;58:771–776.
- Brown S. PDT comes of age [editorial]. In: Brown S, ed. *International Photodynamics: A PDT Forum.* West Sussex, UK: Eurocommunica Publications; 1996:1.
- Schuitmaker JJ, Bass P, Van Leengoed HLLM, Vandermeulen FW, Star WM, Vanzandwijn KN. Photodynamic therapy—a promising new modality for the treatment of cancer. *J Photochem Photobiol B.* 1996;34:3–12.
- Spikes JD. Phthalocyanines as photosensitizers in biological system and for the photodynamic therapy of tumors. *Photochem Photobiol.* 1986;43:691–699.
- van Lier JE. Phthalocyanines as sensitizers for PDT of cancer. In: Kessel D, ed. *Photodynamic Therapy of Neoplastic Disease.* Boca Raton, FL: CRC Press; 1990:279–290.
- Rosenthal I. Phthalocyanines as photodynamic sensitizers. *Photochem Photobiol.* 1991;53:859–870.
- Brasseur N, Ali H, Langlois R, van Lier JE. Biological activities of phthalocyanines, VII: photoinactivation of V-79 chinese hamster cells by selectively sulfonated gallium phthalocyanines. *Photochem Photobiol.* 1987;46:739–744.
- Paquette B, Ali H, Langlois R, van Lier JE. Biological activities of phthalocyanines, VIII: Cellular distribution in V-79 chinese hamster cells and phototoxicity of selectively sulfonated aluminum phthalocyanines. *Photochem Photobiol.* 1988;47:215–220.
- Peng Q, Farrants GW, Madslien K, et al. Subcellular localization, redistribution and photobleaching of sulfonated aluminum phthalocyanines in a human melanoma cell line. *Int J Cancer.* 1991;49:290–295.
- Margaron P, Grégoire MJ, Ščasnář V, Ali H, van Lier JE. Structure–photodynamic activity relationships of a series of 4-substituted zinc phthalocyanines. *Photochem Photobiol.* 1996;63:217–223.
- Margaron P, Madarnas P, Ouellet R, van Lier JE. Biological activities of phthalocyanines, XVII: histopathologic evidence for different mechanisms of EMT-6 tumor necrosis induced by photodynamic therapy with disulfonated aluminum phthalocyanine or Photofrin. *Anticancer Res.* 1996;16:613–620.
- Fingar VH, Wieman TJ, Siegel KA, et al. The effects of photodynamic therapy using zinc phthalocyanines on vessel constriction, vessel leakage and tumor response. *Photochem Photobiol.* 1993;58:251–259.
- van Leengoed HLLM, van der Veen N, Versteeg AAC, Ouellet R, van Lier JE, Star WM. In vivo photodynamic effects of phthalocyanines in a skin fold observation chamber model: role of central metal ion and degree of sulfonation. *Photochem Photobiol.* 1993;58:575–580.
- Chan W-S, Brasseur N, La Madeleine C, van Lier JE. Evidence for different mechanisms of EMT-6 tumor necrosis by photodynamic therapy with disulfonated aluminum phthalocyanine or Photofrin: tumor cell survival and blood flow. *Anticancer Res.* 1996;16:1887–1892.
- Brasseur N, Lewis K, Rousseau J, van Lier JE. Measurement of tumor vascular damage in mice with $^{99\text{m}}\text{Tc}$ -MIBI following photodynamic therapy. *Photochem Photobiol.* 1996;64:702–706.
- Moore JV, West CML, Whitehurst C. The biology of photodynamic therapy. *Phys Med Biol.* 1997;42:913–935.
- Ali H, Langlois R, Wagner JR, Brasseur N, Paquette B, van Lier JE. Biological activities of phthalocyanines, X: synthesis and analyses of sulfonated phthalocyanines. *Photochem Photobiol.* 1988;47:713–717.
- Lecomte R, Cadorette J, Richard P, Rodrigue S, Rouleau D. Design and engineering aspects of a high resolution positron tomograph for small animal imaging. *IEEE Trans Nucl Sci.* 1994;41:1446–1452.
- Lapointe D, Cadorette J, Rodrigue S, Lecomte R. Microvolumetric blood sampler for small animal PET studies [abstract]. *J Nucl Med.* 1997;38:205P–206P.
- Lapointe D, Cadorette J, Rodrigue S, Lecomte R. A microvolumetric blood counter/sampler for metabolic PET imaging of small animals. *IEEE Trans Nucl Sci.* 1998;45:2195–2199.
- Marriott, CJ, Cadorette JE, Lecomte R, Ščasnář V, Rousseau J, van Lier JE. High-resolution PET imaging and quantitation of pharmaceutical biodistributions in a small animal using avalanche photodiode detectors. *J Nucl Med.* 1994;35:1390–1397.